Journal of Hydrology 529 (2015) 1754–1767

Contents lists available at ScienceDirect

Journal of Hydrology

journal homepage: www.elsevier.com/locate/jhydrol

Spatio-temporal validation of long-term 3D hydrological simulations of a forested catchment using empirical orthogonal functions and wavelet coherence analysis

Zhufeng Fang [a,b,*], Heye Bogena [a,b], Stefan Kollet [a,b], Julian Koch [c], Harry Vereecken [a,b]

[a] Agrosphere Institute, Forschungszentrum Jülich GmbH, Germany
[b] Centre for High-Performance Scientific Computing in Terrestrial Systems, HPSC TerrSys, Geoverbund ABC/J, Germany
[c] Department of Geosciences and Natural Resource Management, University of Copenhagen, Denmark

ARTICLE INFO

Article history:
Received 9 April 2015
Received in revised form 3 August 2015
Accepted 7 August 2015
Available online 13 August 2015
This manuscript was handled by Peter K. Kitanidis, Editor-in-Chief, with the assistance of Roseanna M. Neupauer, Associate Editor

Keywords:
3D hydrological simulation
Soil moisture
EOF analysis
Wavelet coherence analysis

SUMMARY

Soil moisture plays a key role in the water and energy balance in soil, vegetation and atmosphere systems. According to Wood et al. (2011) there is a grand need to increase global-scale hyper-resolution water–energy–biogeochemistry land surface modelling capabilities. These modelling capabilities should also recognize epistemic uncertainties, as well as the nonlinearity and hysteresis in its dynamics. Unfortunately, it is not clear how to parameterize hydrological processes as a function of scale, and how to test deterministic models with regard to epistemic uncertainties. In this study, high resolution long-term simulations were conducted in the highly instrumented TERENO hydrological observatory of the Wüstebach catchment. Soil hydraulic parameters were derived using inverse modelling with the Hydrus-1D model using the global optimization scheme SCE-UA and soil moisture data from a wireless soil moisture sensor network. The estimated parameters were then used for 3D simulations of water transport using the integrated parallel simulation platform ParFlow-CLM. The simulated soil moisture dynamics, as well as evapotranspiration (ET) and runoff, were compared with long-term field observations to illustrate how well the model was able to reproduce the water budget dynamics. We investigated different anisotropies of hydraulic conductivity to analyze how fast lateral flow processes above the underlying bedrock affect the simulation results. For a detail investigation of the model results we applied the empirical orthogonal function (EOF) and wavelet coherence methods. The EOF analysis of temporal–spatial patterns of simulated and observed soil moisture revealed that introduction of heterogeneity in the soil porosity effectively improves estimates of soil moisture patterns. Our wavelet coherence analysis indicates that wet and dry seasons have significant effect on temporal correlation between observed and simulated soil moisture and ET. Our study demonstrates the usefulness of the EOF and wavelet coherence methods for a more in-depth validation of spatially highly resolved hydrological 3D models.

1. Introduction

More reliable weather and climate models for the prediction of water, energy and CO_2 transport are needed to better support the management of natural resources. For the improvement and validation of such models, a better understanding of the processes and interdependencies within and between soil, vegetation and the atmosphere are urgently needed (Wood et al., 2011). Soil moisture is the most significant variable in the soil-vegetation-atmosphere continuum due to its important role in the exchange of water and energy at the soil surface. Fast lateral flow under gravitational forces (interflow) can facilitate fast redistribution of soil water in hillslopes during intensive precipitation events (e.g. Hopp et al., 2011; Zhang et al., 2011). However, this important hydrological flux is still poorly understood, because it is difficult to measure and quantify (e.g. Weiler and McDonnell, 2007; Bachmair and Weiler, 2012). Recently, it was recognized that interflow is also very important for understanding the spatial and temporal variability of biogeochemical fluxes and trace gas emissions (e.g. Groffman et al., 2009; Tang et al., 2014). According to Ghasemizade and Schirmer (2013) interflow processes are mainly controlled by factors depending on topography, geology, soil

* Corresponding author at: Agrosphere Institute, Forschungszentrum Jülich GmbH, Germany.
E-mail address: z.fang@fz-juelich.de (Z. Fang).

http://dx.doi.org/10.1016/j.jhydrol.2015.08.011
0022-1694/

properties, rainfall, and vegetation. Previous modelling studies suggest that interflow processes are governed by hillslope characteristics, such as the depth to bedrock and the presence and connectivity of preferential flow pathways (e.g. Tromp-van Meerveld and McDonnell, 2006; Weiler and McDonnell, 2007; Bachmair and Weiler, 2012). Cornelissen et al. (2014) conducted a 3D simulation of the Wüstebach catchment, located in the Eifel mountain range in Germany, using the hydrological model HydroGeoSphere with the aim to explore forest catchment spatiotemporal soil moisture variability. They showed that sharply rising discharge peaks resulting from fast lateral subsurface flow could not be reproduced, because of simplified spatially homogeneous soil and bedrock properties. This demonstrates the need for considering the effect of heterogeneity and anisotropy of soil hydraulic parameters better simulate the mass and energy dynamics in mountainous forest catchment. Recently, an analysis of preferential flow occurrences in the Wüstebach catchment was presented (Wiekenkamp et al., submitted for publication). According to this study, fast interflow can occur in Wüstebach especially after strong precipitation events. In addition, the study of Stockinger et al. (2014) suggests, that during times of high catchment wetness, hillslopes are getting connected to the riparian zone via interflow processes. In this study, we investigated how these interflow processes can be represented in the framework of numerical modelling.

Another aspect, which is often overlooked in hydrological modelling studies, is the litter layer in forest ecosystems, mainly due to limitations in the direct measurement of forest floor processes. An exception is the study of Schaap et al. (1997), who investigated the moisture dynamics of a coniferous forest floor and derived hydraulic properties of the litter layer. Recently, Bogena et al. (2013) used these hydraulic properties to simulate temporal water dynamics in the litter layer of the forest catchment Wüstebach demonstrating its importance for soil moisture assessment.

A parallel, three-dimensional, variably saturated water transport code ParFlow (Ashby and Falgout, 1996; Maxwell et al., 2014) was developed for simulating large-scale, high-resolution flow problems. The ParFlow platform was extended to consider energy and mass balance at the land surface by incorporating the Common Land Model (CLM; (Dai et al., 2003)) into ParFlow (Kollet and Maxwell, 2008; Maxwell and Miller, 2005). However, due to the limitation of availability of in-situ dataset measurement, it was usually difficult to validate the results of long-term, high-resolution surface-subsurface flow problems, especially for the forested catchments.

Spatial and temporal patterns of fluxes and states in the soil-vegetation-atmosphere continuum are inseparably intertwined, resulting in complex feedbacks and system responses on different spatial and temporal scales (Simmer et al., 2015). One useful way to investigate the spatiotemporal relations between water budget components and soil moisture is applying the method of empirical orthogonal functions (EOF) (Graf et al., 2014; Kim and Barros, 2002; Liu, 2003; Syed et al., 2004; Jawson and Niemann, 2007; Schmidt et al., 2008). However, the EOF analysis has not yet been used for the spatio-temporal validation of a 3D simulation of soil moisture patterns. Very recently, Koch et al. (2015) applied the EOF-analysis in a novel manner for the spatial validation of a distributed hydrological model with observed satellite based land surface temperature data and Mascaro et al. (2015) utilized EOFs to analyze results from a high-resolution distributed hydrologic simulation. Wavelet analysis has been applied in catchment studies (Lauzon et al., 2004), model validation (Schaefli and Zehe, 2009), field-scale time series (Vargas et al., 2010), and also in combination with EOF analysis (Parent et al., 2006). To our knowledge, a combined EOF and wavelet analysis to explore modelled spatiotemporal patterns of soil water content, runoff and evapotranspiration has not been applied so far on catchment scale.

The objective of this study is to perform high resolution 3D water flow simulations of a forested headwater catchment using the Parflow-CLM model. We selected the Wüstebach catchment as the study area for this study to utilize the comprehensive validation data sets from atmospheric, pedological and hydrological monitoring equipment installed in the framework of the TERENO and SFB/TR32 projects (Bogena et al., 2010, 2015). This integrated data ideally suited for the analysis of pattern in soil-vegetation-atmosphere systems (Simmer et al., 2015) and of the linkage between hydrological and atmospheric processes in complex environments such as forest ecosystems. In our study, we conducted high-resolution hydrological simulations of a complex forest catchment using the Parflow-CLM model and evaluated different parameterization schemes. For the evaluation with employed a combination of EOF and wavelet analysis to enable a more in-depth analysis of the model performance. This study was to answer the following research questions: (1) how can fast lateral flow above the bedrock be represented in a 3D Richards-equation based model; (2) how will different representations of heterogeneity of soil properties affect the performance of a 3D hydrological model; and (3) what is the value of EOF and wavelet coherence analysis for the spatiotemporal validation of hydrological models.

2. Materials and methods

2.1. The experimental test site

This research was conducted in the Wüstebach catchment (Fig. 1), a 38.5 ha large experimental test site of the TERENO Eifel/Lower Rhine Valley Observatory (Zacharias et al., 2011; TERENO, 2011) located in the National park Eifel. The altitude ranges from 595 m in the north to 628 m in the south. The average slope is modest (3.6%) with maximum values near the river (up to 10.4%). The geology is dominated by fractured Devonian shales with occasional sandstone inclusions and a hydraulic conductivity on the order of 10^{-9} to 10^{-7} m/s (Graf et al, 2014). The bedrock is overlain by a periglacial solifluction layer of about 1–2 m thickness, in which typical soil types have developed. Cambisols and Planosols are mainly located on hill slopes, whereas Gleysols and half-bogs have been developed in the riparian zone under the influence of groundwater (Fig. 1). The prevailing soil texture is silty clay loam with a medium to high fraction of coarse material, and the litter layer has a thickness between 3 and 5 cm (Richter, 1995). More than 90% of the forest is comprised of Norway spruce trees planted in 1946 (Etmann, 2009), with a typical canopy height of about 25 m. The test site belongs to the temperate climate zone with a mean temperature of about 7 °C and a long-term mean precipitation rate of 1310 mm/a for the period 1981–2010.

We made use of long-term soil moisture data from a wireless senor network installed in the Wüstebach catchment consisting of 150 sensor nodes (Bogena et al., 2010), each equipped with four ECH2O EC-5 and two 5TE sensors (Decagon Devices, Inc.) To cover the test site area the sensor locations were distributed using a raster configuration with a resolution of 60 m. Additional locations were randomly located within each raster cell to achieve a wide range of distance classes. Soil moisture is measured in three depths (5, 20 and 50 cm) with a temporal resolution of 15 min (Bogena et al., 2010). Calibration of the sensors is explained in detail in Rosenbaum et al. (2012). We followed Cornelissen et al. (2014), who used EMI (electromagnetic imaging) data to identify representative sensor network locations and to remove outliers. Accordingly, soil moisture observations at 104 sensor nodes were

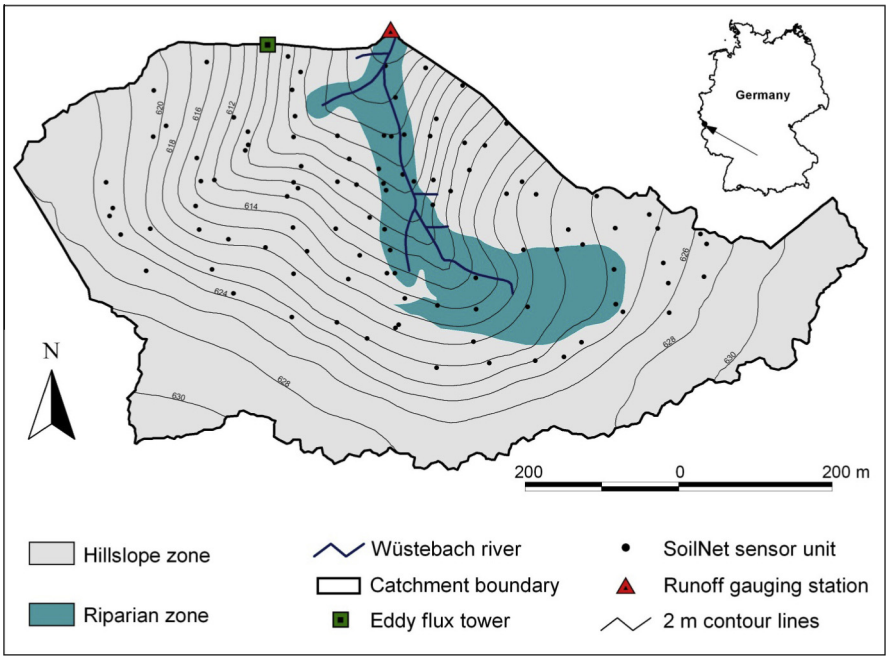

Fig. 1. Map of the instrumentation of the Wüstebach experimental catchment with two soil types.

used in the study for the inverse estimation of hydraulic parameters and for comparison with simulations results. The eddy covariance tower provided the actual ET data used for model validation, see (Bogena et al., 2015) for a detailed description of the measurement technique.

2.2. The ParFlow-CLM simulation platform

The core of the ParFlow-CLM simulation platform used in this study is the ParFlow model (Ashby and Falgout, 1996), which is a parallel, three-dimensional, variably saturated water transport code that is especially suitable for large-scale, high-resolution flow problems. ParFlow makes use of advanced numerical solvers and multigrid preconditioners for massively parallel computer environments. It uses a sophisticated octree-space partitioning algorithm to depict complex structures in three-space, such as topography, different hydrologic facies, and watershed boundaries. ParFlow simulates the three-dimensional variably saturated subsurface flow by solving the Richards equation:

$$\frac{\partial \theta}{\partial t} = \nabla \cdot K(\psi)\nabla\psi + \frac{\partial K(\psi)}{\partial z} \quad (1)$$

where θ (–) is the volumetric moisture, K is hydraulic conductivity (L/T), and ψ is the hydraulic head (L).

Advanced boundary conditions, such as free-surface overland flow, afford the simulation of hillslope runoff and channel routing in an integrated fashion. Distributed surface roughness can be applied to honor different land cover types in the watershed.

The ParFlow platform was extended to consider energy and mass balance at the land surface by incorporating the Common Land Model (CLM; (Dai et al., 2003)) into ParFlow (Kollet and Maxwell, 2008; Maxwell and Miller, 2005). This coupled ParFlow-CLM model can quantitatively exchange information between the land surface and the subsurface, such as plant interception, root uptake and evapotranspiration, in an operator splitting approach. For this study, we employed the version v693 of ParFlow-CLM released on July 28, 2014.

2.3. Model setup

The model domain used for the Wüstebach catchment has a size of 1180 m × 74 m and a uniform depth of 1.6 m, which corresponds to the averaged measured soil depth. In addition, following Bogena et al. (2013) a litter layer was considered with a uniform depth of 0.05 m. We used the DEM of the Land Surveying Office of North Rhine-Westphalia with a spatial resolution of 10 m to spatially discretize the model domain and to assign slope values to each grid. The vertical resolution of the model domain was set to 0.025 m. The total number of spatially uniform grids in the model domain was 118 × 74 × 66. The flow direction grid was generated using GRASS software. We utilized the terrain following grid (TFG) method (Maxwell, 2013) to decrease the number of vertical grid cells.

The CLM model is used to define the top boundary of the ParFlow-CLM simulation platform. We used hourly information on global radiation, precipitation rate, air temperature, wind speed, air pressure, and specific humidity from the Kalterherberg climate station of the German Weather Service (located 9.6 km west of the Wüstebach catchment) to force the CLM model. This climate station is well representative for our test site as demonstrated in the study of Graf et al. (2014). The lateral boundary condition was set as a constant head of −0.88 m, which corresponds to the average depth of observed water table in the area. No flux boundary condition was chosen for the bottom of the model domain since the bedrock of the Wüstebach catchment has a very low permeability, and deep drainage into the bedrock was found to be negligible (Graf et al., 2014).

The soil profile was differentiated into four different soil horizons with specific hydraulic properties following Bogena et al. (2013): a soil covering litter layer (+0.05–0 m), a top A horizon (0–0.1 m), an intermediate B horizon (0.1–0.4 m), and a C horizon (0.4–1.6 m) overlaying the bedrock (see Fig. 2).

Soil hydraulic properties were parameterized using the van Genuchten – Mualem model (VGM):

$$\theta(h) = \begin{cases} \theta_r + \frac{\theta_s - \theta_r}{(1+|\alpha h^n|)^m}, & h < 0 \\ \theta_s, & h \geqslant 0 \end{cases} \quad (2)$$

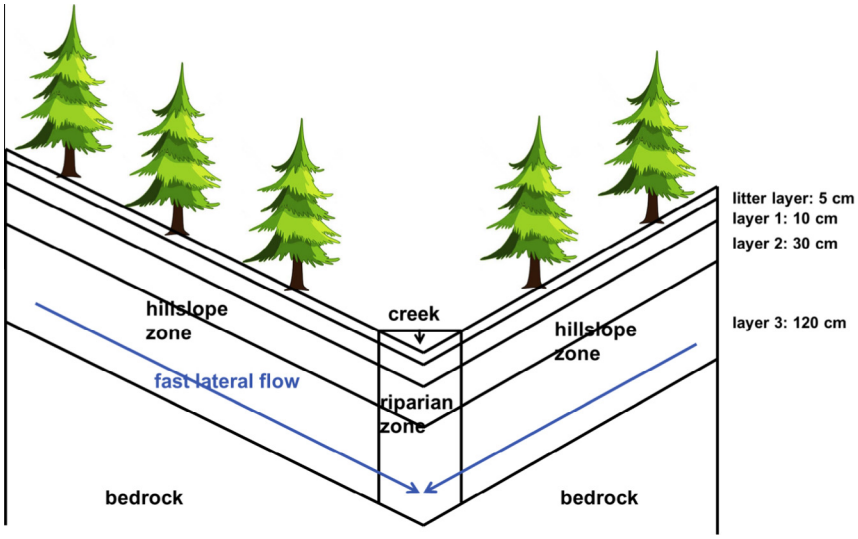

Fig. 2. Schematic model of the Wüstebach catchment.

$$K(h) = K_s S_e^{0.5}\left[1 - \left(1 - S_e^{\frac{0.5}{m}}\right)^m\right]^2 \quad (3)$$

$$S_e = \frac{\theta - \theta_r}{\theta_s - \theta_r} \quad (4)$$

$$m = 1 - \frac{1}{n} \quad (5)$$

where K_s is the saturated soil hydraulic conductivity (m day^{-1}), S_e is the effective saturation, θ_r and θ_s (m^3 m^{-3}) represent the residual and saturated SWC, α (m^{-1}), n and m (both dimensionless) are parameters for fitting the soil water retention function. Due to lack of measurements, the hydraulic parameters θ_r, α, n, and K_s were estimated for each soil layer using inverse modelling, see Section 2.4. The parameter θ_s was fixed to the maximum value of the observed soil moisture during the study period for each soil layer. This simple approach is valid, because high precipitation amounts have led to an observed saturation of the whole soil profile several times during the study period.

Following Bogena et al. (2013), we adopted the study of Schaap et al. (1997) to define appropriate values for the parameters θ_r, α, n and K_s of the litter layer. The paramter θ_s was estimated from the mean porosity of eight litter layer samples collected in the site (Bogena et al., 2013). The corresponding hydraulic parameters used for the ParFlow-CLM simulation are as follows: K_s = 200.0 - cm/day, θ_r = 0, θ_s = 0.87, α = 0.0264 cm^{-1}, and n = 1.286.

The simulation was conducted on hourly time steps for 1216 days from May 1 2010 to April 30 2013, before the deforestation work started (Bogena et al., 2015). A spinup phase from January 1 to April 30, 2010 was conducted with an initial condition of constant head in −2.0 m. Actually, several testing simulation runnings indicated that the initial condition between -0.1 m to 5.0 m gave almost same results after one to two months running. Therefore the spinup phase was fairly effective. The simulations were performed on the high performance computer JUROPA in Centre for High-Performance Scientific Computing in Terrestrial Systems, HPSC TerrSys, Geoverbund ABC/J and clusters of the Forschungszentrum Jülich GmbH. It took around 40–60 h for the 3-year simulations to complete. Considering its long term and the complicated interacted atmospheric-hydrological system in this study, such computational times are well accepted.

2.4. Inverse estimation of hydraulic parameters

Soil hydraulic parameters can be determined either by direct or indirect methods. In case of direct methods, the hydraulic parameters are estimated by fitting the water retention and unsaturated hydraulic conductivity curve to experimental data obtained from soil cores in the laboratory. However, soil heterogeneity requires that a very large number of samples would be needed to adequately represent the variability of soil properties in the study area, which is very expensive and time consuming. Since measured time series of soil moisture at several depths are available as for this study, inverse modelling may be an appropriate alternative to obtain in-situ soil hydraulic parameter estimates (e.g. Vrugt et al., 2003; Zhang et al., 2004). However, inverse modelling is computationally demanding and not feasible for 3D models based on the Richard's equation even in the presence of high performance computing facilities. Recently, Qu et al. (2014) showed that most of the spatial variability of soil moisture in the Wüstebach catchment can be described using a 1D vertical Richard's equation approach. Thus, we followed the approach of Bogena et al. (2013) and used an inverse HYDRUS-1D model (Simunek and van Genuchten, 2008) to estimate the parameters of the Mualem-van Genuchten model.

The initial soil profile for HYDRUS 1-D was set to be saturated, and a 6-month spin up period with actual meteorological data was applied. Therefore, the simulation period was from 1 July 2009 to 30 April 2013. The reference potential evapotranspiration (ET_0) was computed by the Penman-Monteith equation (Allen et al., 1998). Potential evaporation (E) and transpiration (T) were separated based on the leaf area index (LAI):

$$T = ET_0(1 - e^{-kLAI}) \quad (6)$$

$$E = ET_0 e^{-kLAI} \quad (7)$$

where k is a parameter (–) that governs the radiation extinction of the canopy. Given that the study area was homogenously covered by Norway spruce forest, it was found that a k value of 0.75 and a LAI value of 4 are appropriate (Bogena et al., 2013).

The root distribution was set to decrease linearly from maximum value at the soil surface to zero at 50 cm depth with a unit gradient. Root water uptake was computed by the Feddes approach (Feddes et al., 1976) implemented in HYDRUS-1D. The lower boundary was set to be three different types for comparison: free drainage (FD), constant head (CH), and seepage face (SF).

We discretized the soil profile in HYDRUS-1D in the same way the ParFlow-CLM model (three soil horizons plus a litter layer of organic material on top of the soil) and applied the global optimization algorithm SCE-UA (Duan et al., 1994) to estimate

VGM parameters. We used spatially averaged SoilNet soil moisture data for three depths (5, 20 and 50 cm) from January 1 2009 and April 30 2013 to estimate soil hydraulic parameters for each of the three soil horizons (Fig. 2). The litter layer was parameterized in the same way as the ParFlow-CLM model.

2.5. Model scenarios

Two scenarios were simulated in order to illustrate how we can improve model performance by introducing anisotropy (different parameter values at different directions) and heterogeneity (different parameter values at different points) using Parflow-CLM. During strong precipitation events the soils in the study area often reached saturation, which activated fast lateral water flow pathways above the impermeable bedrock (Rosenbaum et al., 2012; Stockinger et al., 2014). We mimic the fast interflow process by assuming a strong horizontal anisotropy in the bottom soil layer (C horizon). Due to the high computational demand of ParFlow-CLM required for a 3-year simulation period, it was impossible to inversely estimate the optimal horizontal K_s value. Therefore, we investigated different scaling factors for the horizontal component of K_s to find the best representation of the interflow process in the Wüstebach catchment (modelling scenario SC1). We used a series of the scaling factors of anisotropy (10, 20, 40, and 80, respectively). During this study, the vertical K_s value was kept unchanged and isotropy in K_s in the upper two soil horizons was assumed because fast lateral flow typically occurs above the bedrock interface (e.g. Lin, 2006; Hopp and McDonnell, 2009; Uchida et al., 2005). To evaluate the quality of the different scenarios we compared observed and simulated runoff, evapotranspiration, and soil moisture time series and used the root mean square error (RMSE) and Nash-Sutcliffe efficiency (NSE) as simulation quality criteria. The scaling factor that resulted in the best simulation results was used for all following simulations.

In a second modeling scenario (SC2), we investigated the effect of spatial heterogeneity of soil porosity on the simulation results. We considered a homogeneous case (SH1) and heterogeneous case (SH2), in which soil porosity was fully distributed. The distributed porosity was determined from the maximum observed soil moisture at 104 monitoring locations, then interpolated to the whole domain using a Geographical Information System (ArcGIS, Esri, Redlands, CA), and subsequently clustered into 6 groups per layer (Fig. 3, Table 1).

2.6. Validation data

The validation of the simulation results was performed using observed states and fluxes in the Wüstebach catchment (i.e. soil moisture, runoff, and evapotranspiration) in daily resolution from January 2009 to May 2013. Using the same data, Graf et al. (2014) were able to close the local water balance of the Wüstebach catchment. Thus, this comprehensive data set is ideally suited for the validation of hydrological models like ParFlow-CLM.

2.7. Empirical Orthogonal Function (EOF) analysis

We employed the EOF method (Perry and Niemann, 2008) for a detailed analysis of the spatiotemporal pattern of simulated and observed soil moisture. Both observed and simulated soil moisture data sets contained 312 variables (104 monitoring points by 3 layers). Thus, we applied the EOF to the matrix of 312 measurement locations and 1096 days. This formed a 312×1096 matrix Y_0 with the soil moisture data, the rows representing the 312 measurement locations and the columns representing the 1096 measurement days. Then a new 312×1096 matrix Y was formed, each column of the matrix was average to zero with a prior removal of the means. Matrix Y can be expressed as a linear combination of new, statistically independent (orthogonal) columns Y' and their loadings (eigenvectors) E in matrix notation:

$$Y = Y' \times E^T \tag{8}$$

where the superscript ^{T} indicates the matrix transpose. The matrix Y' contains the EOFs that can be used to create spatial patterns through interpolation. The first column of Y' describes as much as possible of the variance of Y, and can be used together with the first row of E^T as a memory-saving representation of a noise-reduced version of Y; the second and any further column of Y' describe as much as possible of the remaining variance.

As for the purpose of model validation, we followed the approach of Graf et al. (2014) and used only the first two EOF and loading time series. That means we only used the first two columns of Y', Y'^*, with the largest two variance of Y, and the first two eigenvectors E^* to express a reconstructed 312×1096 matrix Y^* in Eq. (9):

$$Y^* = Y'^* \times E^{*T} \tag{9}$$

Then the reconstructed soil moisture matrix y^r was calculated using:

$$y^r_{ij} = y^*_{ij} + \overline{y_{0i}} \tag{10}$$

where $\overline{y_{0i}}$ refers to the prior removal of the means.

The advantage of EOF analysis is that the spatiotemporal pattern of soil moisture can be represented by a largely reduced number of variables (from 312×1096 to 2×1096). Following Graf et al. (2014), we focus in our validation analysis on the loadings EOF1 and EOF2 because they contain most of the soil moisture pattern information (see Chapter 3.6).

2.8. Wavelet coherence analysis

Wavelet analysis has been applied in catchment studies (Lauzon et al., 2004), model validation (Schaefli and Zehe, 2009), field-scale time series (Vargas et al., 2010), and in combination with EOF analysis (Parent et al., 2006). The continuous wavelet transform of a time-dependent variable $y(t)$ for a specific location along the time axis τ and a specific time scale s is given by Eq. (11) (Si, 2008):

$$W(s,\tau) = \int_{-\infty}^{\infty} y(t) \frac{1}{\sqrt{s}} \varphi^* \left(\frac{t-\tau}{s} \right) dt \tag{11}$$

where φ^* is the complex conjugate of the mother wavelet φ which can be selected from a variety of functions. In this study we used the Morlet wavelet as the wavelet function. Two kinds of wavelet analysis were applied in our study: The global wavelet power spectrum analysis and the cross-wavelet spectrum analysis. The global wavelet power is calculated by averaging the wavelet powers over the localized time instances using:

$$\overline{W^2}(s) = \frac{1}{N} \sum_{n=0}^{N-1} |W_n(s)|^2 \tag{12}$$

Similarly to Fourier analysis (e.g., Mauder et al., 2007), the wavelet transforms of two simultaneous samples variables can be used to compute the cross-wavelet spectrum. The cross-wavelet spectrum of two time series x and y can be calculated using:

$$W^{xy}_n(s) = W^x_n(s) W^y_n * (s) \tag{13}$$

where $W^x_n(s)$ and $W^y_n(s)$ refer to the wavelet transform of time series x and y, respectively. Detailed descriptions of wavelet coherence methods are given in (Torrence and Compo, 1998; Grinsted et al., 2004; Si, 2008; Rahman et al., 2014).

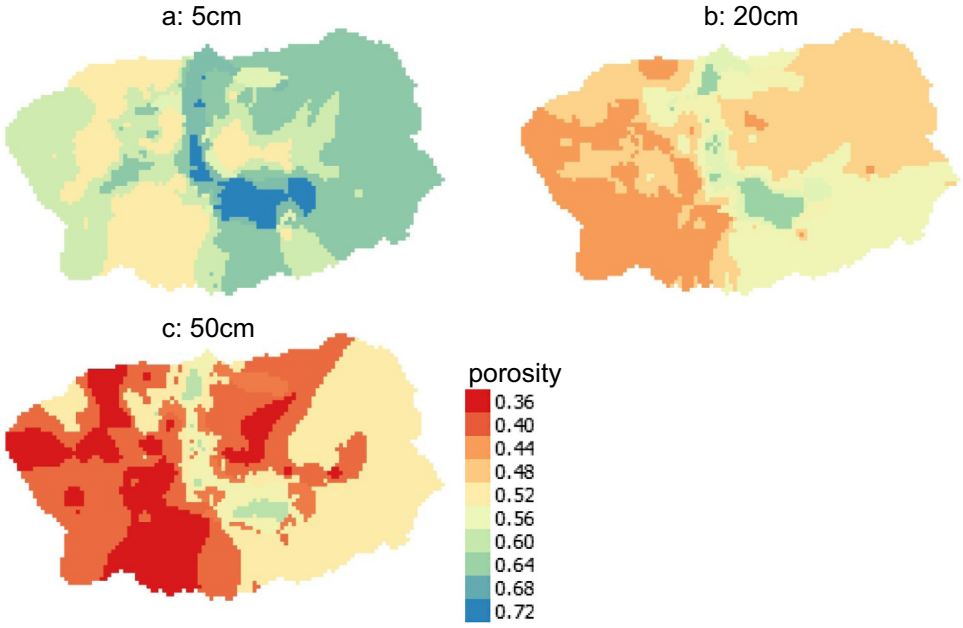

Fig. 3. Estimated porosity distributions for three soil layers (0–10 cm, 10–40 cm, and 40–160 cm, respectively).

Table 1
Distributed porosity θ_s.

Hillslope (1)	Porosity_5 cm	Porosity_20 cm	Porosity_50 cm
Low	0.52	0.44	0.36
Medium	0.59	0.49	0.41
High	0.65	0.55	0.52
Riparian (2)	Porosity_5 cm	Porosity_20 cm	Porosity_50 cm
Low	0.57	0.54	0.42
Medium	0.66	0.57	0.54
High	0.72	0.64	0.61

As for the purpose of model validation, we followed the simplified setup as described in (Graf et al., 2014) to calculate the cross spectrum of simulated and observed variables such as averaged soil moisture, runoff, and evapotranspiration to illustrate the temporal variation in different seasons and time scales. In addition, global wavelet power was also calculated to provide comparison of temporal pattern between simulation and observation of soil moisture. The Matlab code for wavelet coherence analysis used in this study is described in detail in (Grinsted et al., 2004).

3. Results and discussions

3.1. Estimation of hydraulic parameters

Using HYDRUS-1D and SCE-UA, soil hydraulic parameters for the whole model domain were inversely estimated. We tested two bottom boundary conditions: free drainage (FD) and seepage face (SF). The optimized parameters are listed in Table 2. Except for parameter α, both FD and SF boundary condition produced similar parameters. Both cases also produced similar soil moisture dynamics in 5 cm and 20 cm depth, indicated by the close RMSE and NSE values. However, we found that FD gives much better correspondence with observed soil moisture dynamics in 50 cm level compared to the SF boundary condition (RMSE and NSE increased from 0.021 to 0.032 and −0.475 to 0.342, respectively). This indicates that FD is the best boundary condition approximation, although the low permeability of the underlying bedrock in the Wüstebach impedes deep drainage. Clearly, the simple HYDRUS-1D model cannot fully account for the complex soil-bedrock processes at the catchment scale. Nevertheless, given the reasonable simulation results of the HYDRUS-1D model, we selected the VGM parameters estimated using FD boundary condition for the ParFlow-CLM simulations. Further studies with more computational resources are needed to estimate heterogeneous hydraulic parameters from 3-D inverse calibration procedures with more differentiated boundary conditions.

Table 2
Estimated parameters of each layer of the whole domain under bottom boundary of FD and SF from HYDRUS inversion.

	θ_s	K_s (cm/d)	θ_r	α (1/cm)	n	RMSE	NSE
5 cm							
FD	0.57	803.35	0.122	0.010	1.26	0.0494	0.512
SF	0.55	1167.80	0.146	0.022	1.39	0.0483	0.533
20 cm							
FD	0.49	1495.62	0.148	0.010	1.19	0.0277	0.521
SF	0.47	1494.36	0.149	0.031	1.22	0.0279	0.521
50 cm							
FD	0.43	98.76	0.120	0.010	1.21	0.0211	0.3420
SF	0.40	138.52	0.075	0.027	1.27	0.0316	−0.475

3.2. Representation of the interflow process (SC1)

The results of our scenario analysis indicate that ET shows only very low sensitivity to the different K_s anisotropies (Table 3). In contrast, the soil moisture and runoff simulations are more strongly affected by the K_s scaling. For instance, a scaling factor

Table 3
Statistical analysis of comparison of the five anisotropic simulation scenarios.

RMSE	*ET*	Runoff	θ 5 cm	θ 20 cm	θ 50 cm
Isotropy	0.146	0.330	0.113	0.066	0.078
$10 \times K_{sh}$	0.139	0.204	0.065	0.036	0.041
$20 \times K_{sh}$	0.136	0.170	0.059	0.042	0.027
$40 \times K_{sh}$	0.133	0.162	0.070	0.059	0.028
$80 \times K_{sh}$	0.130	0.159	0.088	0.077	0.043

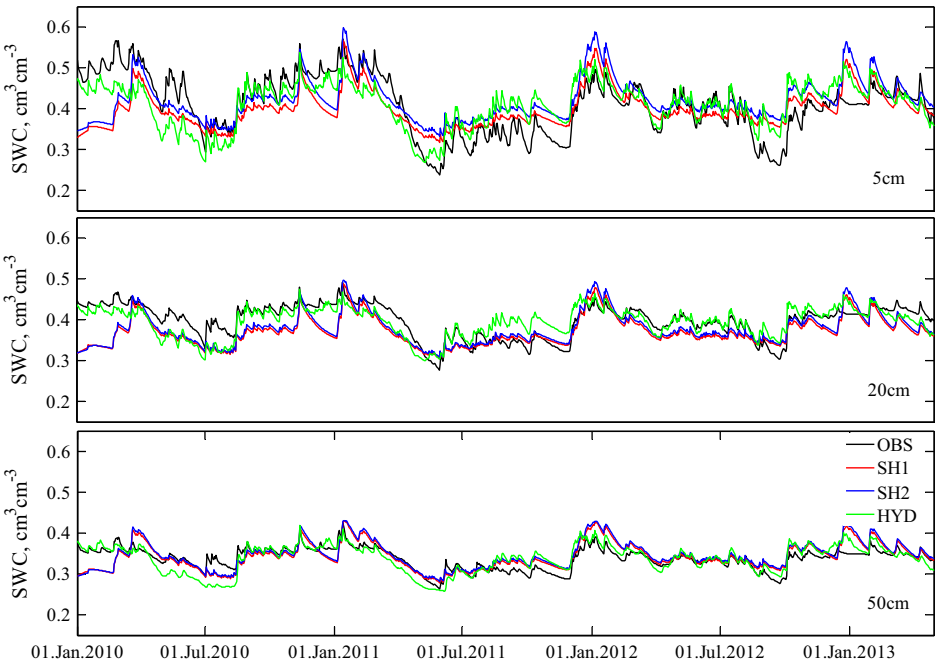

Fig. 4. Observed and simulated daily soil moistures at depths of 5, 20 and 50 cm for different scenarios of spatial heterogeneity and the HYDRUS estimates.

of 20 provided much lower RMSE for soil moisture at both 5 cm and 50 cm depth (0.059 and 0.026, respectively). Increasing horizontal K_s also improved simulated runoff with RMSE reduced from 0.330 to 0.159. As a trade-off, we chose a scaling factor of 20 as a best compromise for the following ParFlow-CLM simulations.

3.3. Effect of heterogeneity

Based on the parameterization described above and the addition of the litter layer, we conducted three simulation cases with different spatial heterogeneity of soil porosity (see Chapter 2.5). Fig. 4 shows a comparison between average simulated and observed soil moisture of the two heterogeneity cases using the ParFlow-CLM model as well as the HYDRUS-1D simulation results. Whereas soil depths of 20 and 50 cm show mainly good correspondence between the simulations and observation, soil moisture simulations at 5 cm depth show distinct deviations from the observations. For instance, ParFlow-CLM overestimated in both cases soil moisture at 5 cm especially after strong precipitation events during the dry seasons. This bias is especially distinct for the dry spring season in 2011, which was also the driest spring season of the last 100 years. Interestingly, HYDRUS-1D was able to simulate this drying-up much better. One possible reason for the bias in the ParFlow-CLM simulations is that the drainage from the catchment is to some extent delayed due to the low topographic gradients in the riparian zone.

Another possible reason for the overestimation during drying phases is the presence of fast vertical bypass flow during strong precipitation events at the Wüstebach site as already suggested by Cornelissen et al. (2014). Recently, Wiekenkamp et al. (submitted for publication) analysed the preferential flow occurrence of the Wüstebach catchment in detail and found that bypass flow occurs especially during intensive rainfall and low antecedent soil moisture conditions induced by hydrophobicity. This finding supports our assumption that soil moisture overestimation is mainly caused by preferential in the topsoil especially during dry periods.

The simulation results of the two heterogeneity cases in terms of RMSE and NSE are presented in Table 4. We found that the ParFlow-CLM model was not very sensitive to the different cases of spatial heterogeneity in soil porosity in terms of ET and runoff. Whereas almost no difference in RMSE was found, NSE indicates that the simulation results were slightly worse in case of heterogeneous soil porosities. In contrast, the soil moisture simulation was clearly positively influenced by the application of heterogeneous soil porosities (the NSE value was 34% higher compared to SH1).

Fig. 5 compares the simulated and observed soil moisture (average of the period between May 2010 and April 2013) for the three depths. The distributed case (SH2) better captures the main features of the observed soil moisture pattern, which is supported by the scatter plots shown in Fig. 6. The Pearson linear correlation (r) increased considerable for all depths (Fig. 6), but especially at 5 cm depth (r increased by ~60%). Clearly, this indicates that distributed information on porosity is important for an accurate simulation of soil moisture pattern.

3.4. Water balance closing

Fig. 7 and Table 5 compare observed and simulated water budgets of the homogeneous and fully distributed cases for the three years simulation period. Both simulation cases gave very similar results. This was expected given the very similar runoff and ET

Table 4
Statistical analysis of comparison of the simulation scenarios SH1 and SH2.

	RMSE					NSE				
	ET	Runoff	θ 5 cm	θ 20 cm	θ 50 cm	*ET*	Runoff	θ 5 cm	θ 20 cm	θ 50 cm
SH1	0.142	0.173	0.064	0.035	0.025	−0.159	0.697	0.087	0.235	0.206
SH2	0.141	0.173	0.052	0.032	0.022	−0.152	0.694	0.388	0.356	0.268

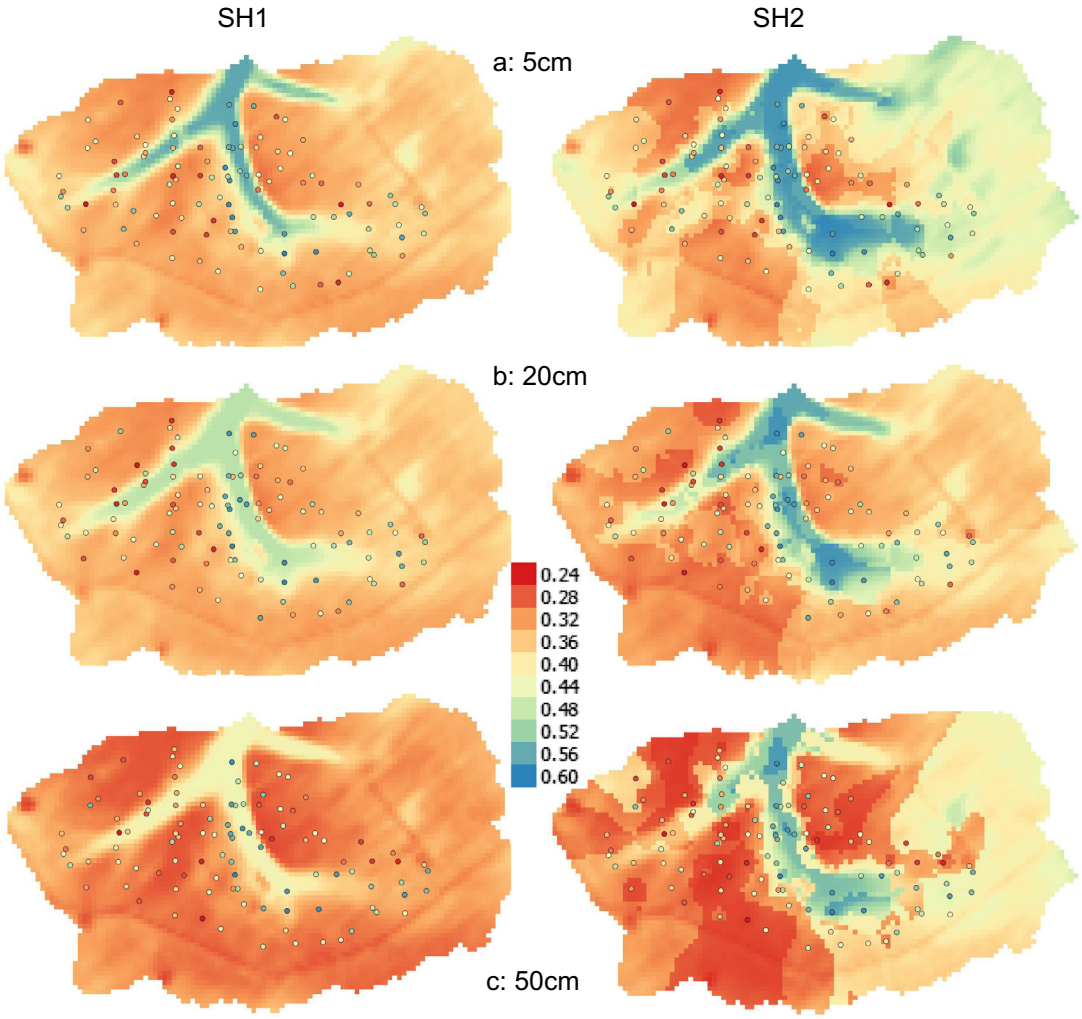

Fig. 5. Observed and simulated soil moisture pattern at 5, 20, and 50 cm depth (3-year average between May 1, 2010 and April 30, 2013) of the two heterogeneity scenarios SH1 and SH2.

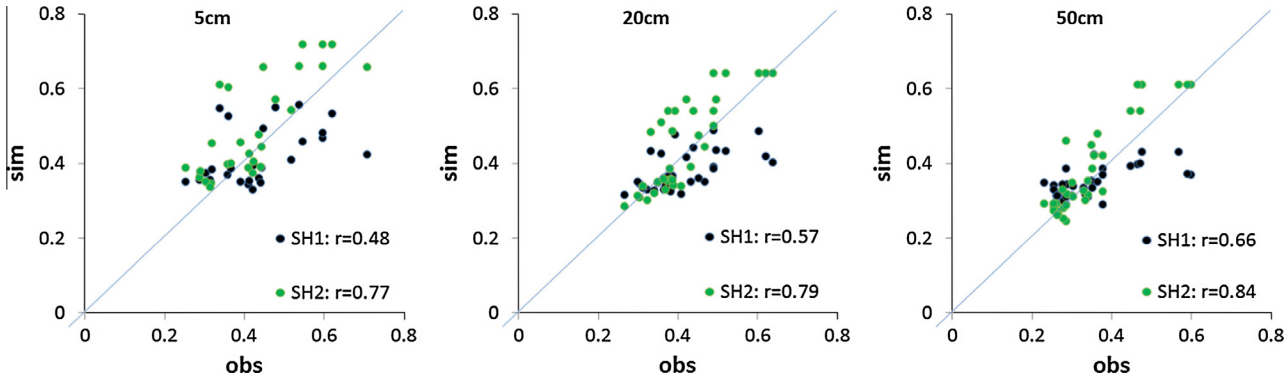

Fig. 6. Scatter plot of observed and simulated 3-year averaged soil moisture of the two heterogeneity scenarios for the three soil depths.

simulation results of both cases (Table 5 shows results of SH2). The total simulated residual $r = P - ET - R$ of the three years period was −27.44 cm in SH1 and −27.10 cm in SH2, of which −18.91 (SH1) and −18.58 cm (SH2) is contributed by the first year. Since the *ET* measurements started on June 23 2010, this data gap had to be filled with a less reliable *ET* model (Graf et al., 2014), which is the main reason for the water budget discrepancy in the first year. In the latter two years, the annual residual of simulation is −3.7 cm and the annual residual percentage $r\% = r/P$ is −3.25%, which is lower than the SH1 case (∼−3.26%), and is acceptable compared to the residual of observation (∼−0.25%).

3.5. EOF analysis

In the following we show results of our EOF analysis focusing on the loadings EOF1 and EOF2 which together describe more than

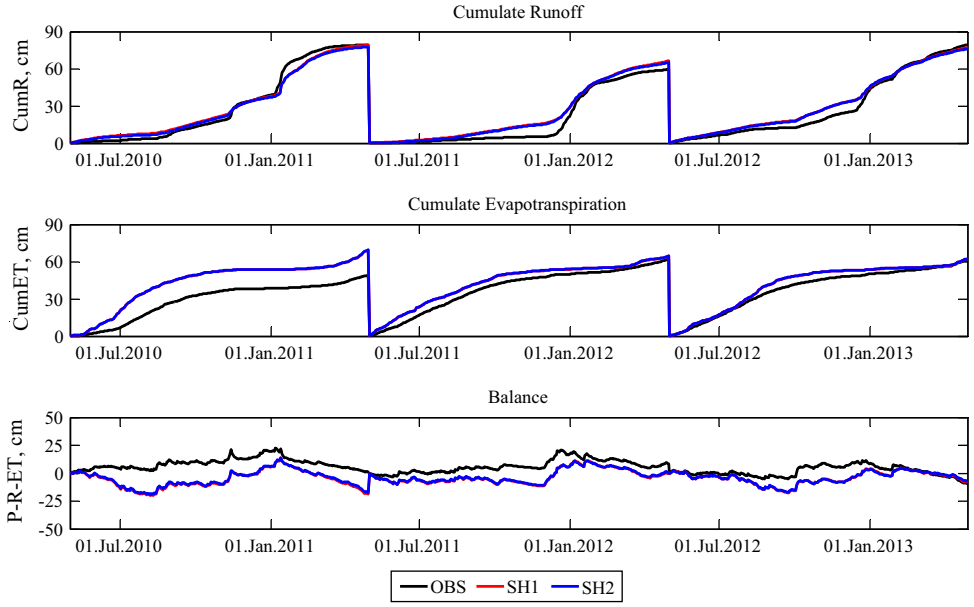

Fig. 7. Observed and simulated water balance components for the period May 2010 – April 2013 using the two heterogeneity scenarios.

Table 5
Observed and simulated water budget elements (precipitation, ET, runoff, residual, and residual percentage) of the Wüstebach catchment for the total study period and annual sub-periods (case SH2).

Unit in cm	*P*	Obs *ET*	Sim *ET*	Obs *R*	Sim *R*	Obs *r*	Obs *r* (%)	Sim *r*	Sim *r* (%)
May 2010 – April 2011	129.57	49.21	69.26	79.15	78.89	1.22	0.94	−18.58	−14.34
May 2011 – April 2012	130.32	62.11	64.54	59.58	66.40	8.62	6.62	−0.62	−0.48
May 2012 – April 2013	131.28	61.29	62.05	79.34	77.13	−9.35	−7.12	−7.89	−6.01
Sum	391.18	172.61	196.53	218.08	218.81	0.49	0.13	−27.10	−6.93

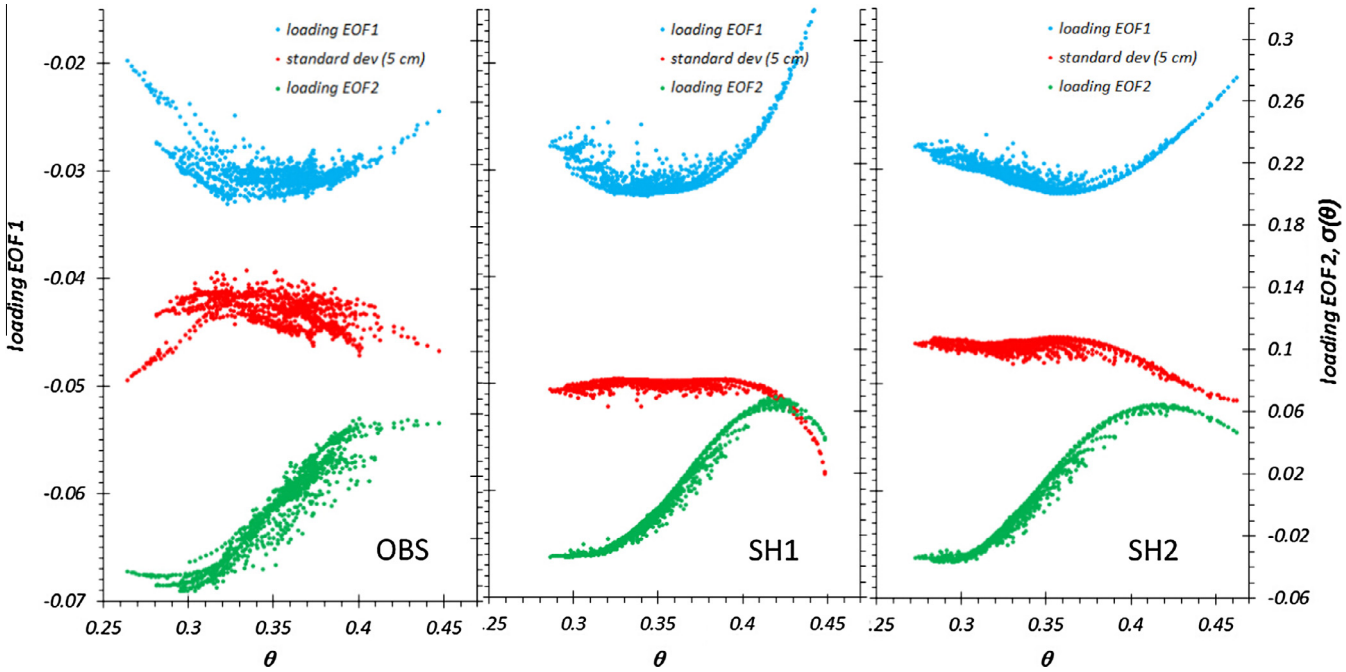

Fig. 8. Loadings of the first two spatial soil moisture EOFs and spatial standard deviation at the 5 cm level against depth-averaged soil moisture θ for the soil moisture observation and ParFlow simulations using the three heterogeneity scenarios.

90% of the total variance of observed soil moisture pattern (Graf et al., 2014). Fig. 8 shows the loadings of EOF1 and EOF2 of the observed and simulated soil moisture time series plotted against spatially averaged soil moisture. From Fig. 8 it becomes apparent that model case SH1 produced more scatter in the loadings of EOF1 as the heterogeneous cases SH2. EOF1 captures the most

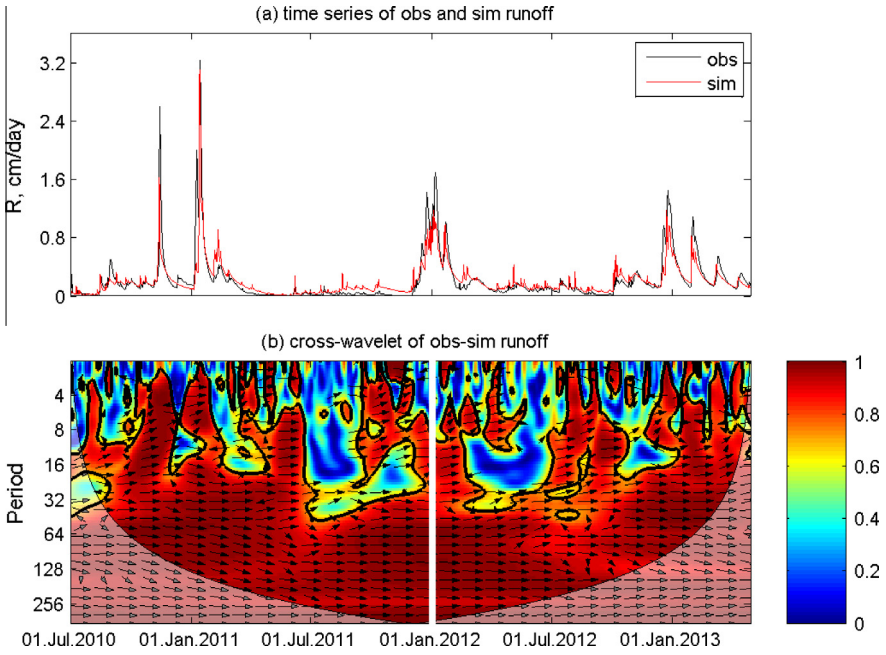

Fig. 9. Cross wavelet coherence analysis for scenario SH2 for runoff. Phase arrows indicate the relative phase relationship between the series (pointing right: delayless correlation; left: anti-correlation; down: observation leading simulation by 90°).

important spatial soil moisture variation in the Wüstebach catchment, which is the soil moisture contrast between the hillslope and riparian zones (Fig. 3). This contrast is mainly produced by the higher soil porosity in the riparian zone due to higher contents of organic matter (Fig. 1).

Both heterogeneity cases are able to reproduce the general pattern of the relationship between EOF2 loadings and mean soil moisture. In contrast to EOF1, the two cases did not produce strong differences in the EOF2 loadings. As the EOF2 loadings represent the second important spatial soil moisture variation, this indicates that the different heterogeneity in porosity did not produced further distinct differences in soil moisture patterns.

The EOFs of the soil moisture simulations also indicate the existence of a turning point θ_t as already found in the study by Graf et al. (2014) suggesting different spatial soil moisture pattern for mean soil moisture below and above θ_t. For example, the loadings of EOF1 show a decreasing trend below θ_t and an increasing trend above θ_t for all cases. In contrast, EOF2 shows an increasing trend below and above θ_t. The value of θ_t case SH1 corresponds with the observations ($\sim$0.35). Introduction of heterogeneity θ_t is shifted very slightly to the wetter part that is negligible.

Fig. 8 also shows the relationship between standard deviation of soil moisture and spatially averaged soil moisture. Clearly, both modelling cases produced less spatial variability in soil moisture

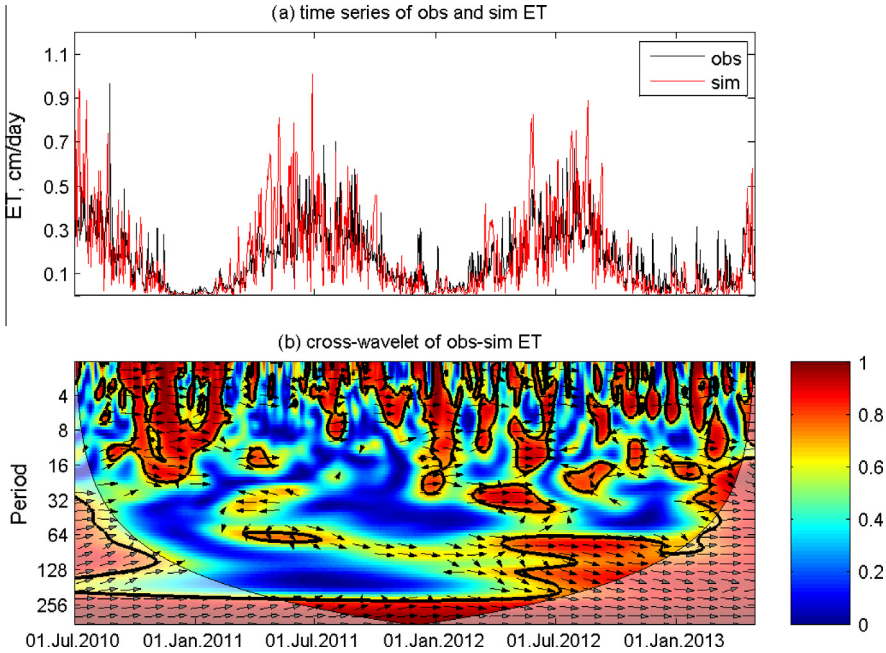

Fig. 10. Cross wavelet coherence analysis for scenario SH2 for ET. Phase arrows indicate the relative phase relationship between the series (pointing right: delayless correlation; left: anti-correlation; down: observation leading simulation by 90°).

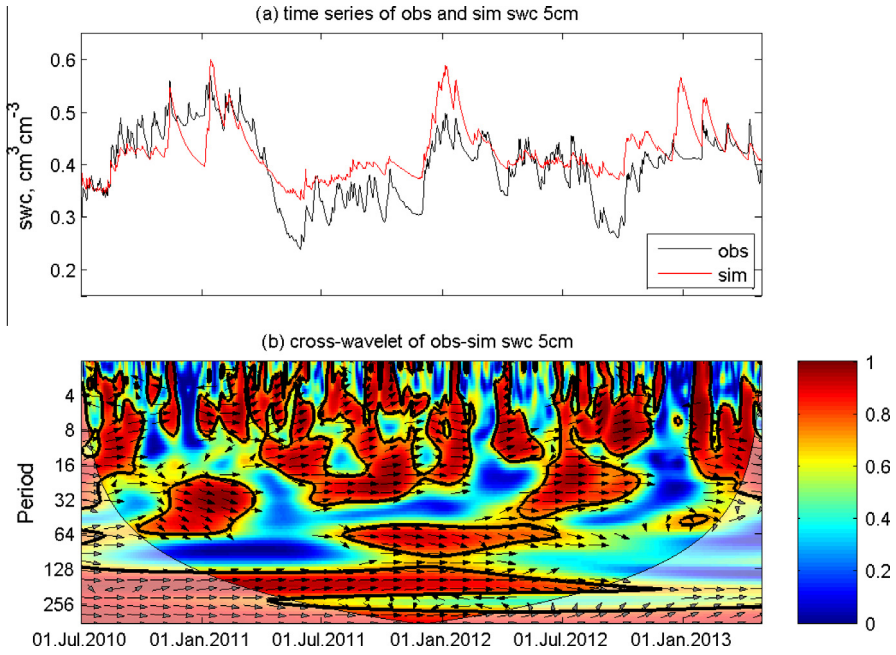

Fig. 11. Cross wavelet coherence analysis for observed and simulated soil moisture at 5 cm depth (case SH2). Phase arrows indicate the relative phase relationship between the series (pointing right: delayless correlation; left: anti-correlation; down: observation leading simulation by 90°).

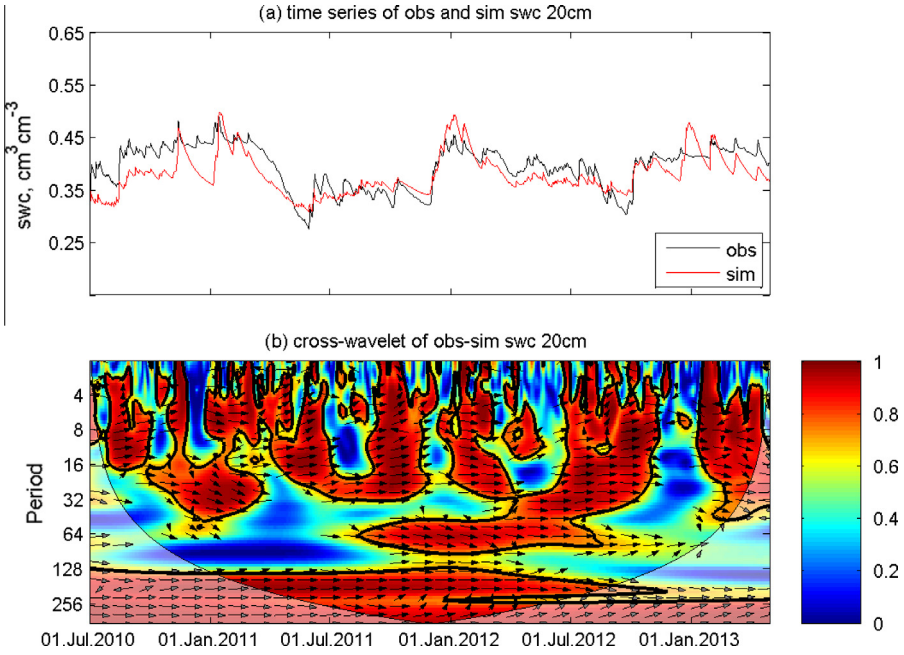

Fig. 12. Cross wavelet coherence analysis for observed and simulated soil moisture at 20 cm depth (case SH2). Phase arrows indicate the relative phase relationship between the series (pointing right: delayless correlation; left: anti-correlation; down: observation leading simulation by 90°).

compared to the observations. Standard deviation (STD) of scenario case SH1 is 32.0% lower and STD of scenario case SH2 is 14.8% lower compared to STD of the observations (~0.14). This is not surprising given the fact that the heterogeneity of the vegetation cover is not represented in the modelling. Interestingly, both cases did not reproduce the decrease in spatial variability towards the dry end. The main reason for this discrepancy is a generally longer lasting wetness contrast between the hillslope and riparian zones in the soil moisture simulations. For instance, the soil moisture observations indicated a dry-out of the riparian zone during the extremely dry spring season 2011, which was not reproduced by the ParFlow-CLM model (see Fig. 4).

The ParFlow-CLM simulation also produced less scatter in the STD versus mean soil moisture relationship. As discussed by Rosenbaum et al. (2012) this scattering is the result of complex hysteresis loops at the event scale. After strong rainfall events, STD increases sharply indicating strong spatial variability in infiltration intensity due to small scale heterogeneities in soil properties and vegetation density. Since both soil and vegetation properties are homogeneous (expect for soil porosity for case

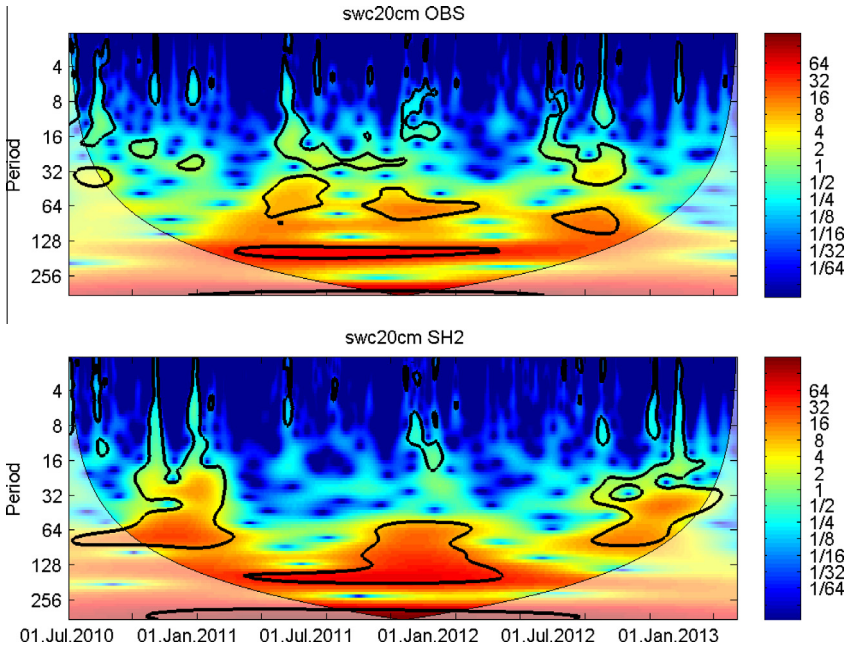

Fig. 13. Power spectrum of observed and simulated (case SH2) soil moisture at 20 cm.

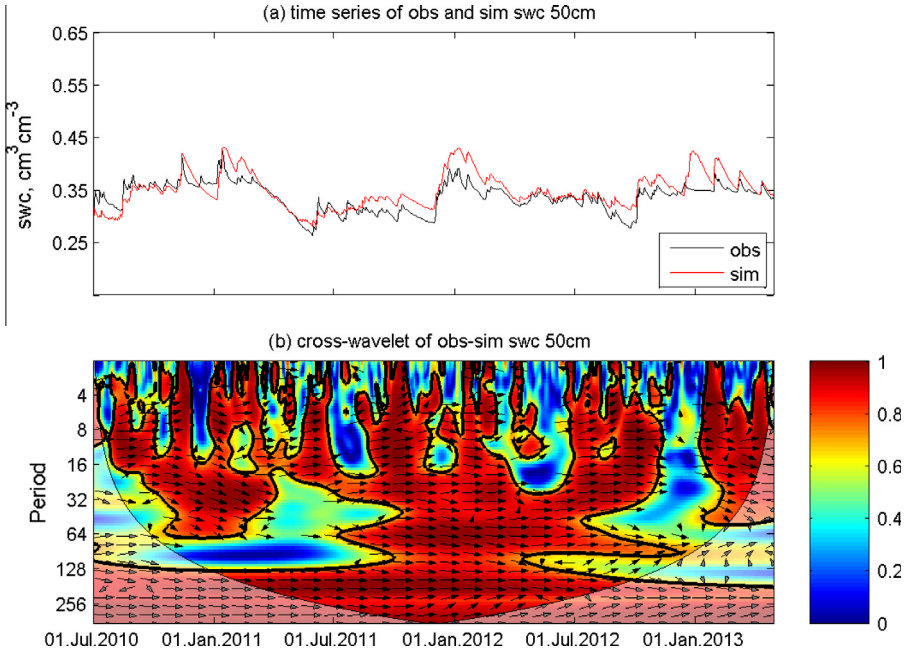

Fig. 14. Cross wavelet coherence analysis for scenario SH2 for soil moisture at 50 cm. Phase arrows indicate the relative phase relationship between the series (pointing right: delayless correlation; left: anti-correlation; down: observation leading simulation by 90°).

SH2), it is not surprising that the STD versus mean soil moisture relationship shows less scattering.

3.6. Wavelet coherence analysis

In the following we present the results of the cross-wavelet coherence analysis using observed and simulated runoff, ET and soil moisture time series. Since both heterogeneity cases produced similar temporal dynamics in terms of catchment scale states and fluxes we focus on case SH2. Fig. 9 presents the time series and the cross wavelet coherence plot of observed and simulated runoff. For the wavelet coherence plot it become apparent that good agreement between observed and simulated runoff exist especially for longer time scales, i.e. larger than one month, with R^2 being mostly larger than 0.9 throughout all the three years periods. Some breakdowns in coherence can be especially observed for shorter time scales less than 15 days. High coherence exists during very wet seasons, e.g. from October 2010 to January 2011 and from January to March 2012, and during distinct runoff events. Taking January 1 2012 as an example for a wetting period, high correlation exists for time scales larger than 15 days indicating that simulated and observed runoff are in good agreement. This is also confirmed by the almost uniform rightward arrowheads indicating delayless correlation.

The cross-wavelet coherence plot shown in Fig. 10 reveals generally lower coherence between observed and simulated evapotranspiration compared to runoff. For the dry season from March to June 2011, coherence is especially low and with presence of anti-correlation (leftward arrow) with a time scale around 30 days. On the other hand, during the wet season from April to December 2012, zones of high coherence exist with time scales larger than 60 days. These findings indicate seasonality of ET simulation accuracy. During wet seasons, the ParFlow-CLM model provides reasonable simulation results, while during dry seasons, delays and anti-correlation in the coherence plots indicate the model is not able to reproduce short-term fluctuations in evapotranspiration.

Figs. 11, 12, and 14 show cross-wavelet coherence plots of observed and simulated soil moisture at 5, 20 and 50 cm depth, respectively. In general, the wavelet coherence plots show similar pattern for all depths. For instance, the plots reveal breakdowns in coherence for shorter time scales (i.e. less than 15 days) for all three depths. Higher coherence exists mainly for time scales larger than 30 days with few delays and anti-correlations. Interestingly, for time scales between 64 and 128 days two distinctive zones of low coherence exist for all soil depths (between January to June 2011, and between August to December 2012, respectively). Both zones of low coherence are coincident with dry periods. The first zone coincident with the extraordinary dry period between March to June 2011 with only 0.24 cm of precipitation during that time.

To further analyze the reason for these breakdowns in coherence, we also present time localized powers wavelet plots taking the soil moisture times series at 20 cm as an example (Fig. 13). In the first period, two distinct zones at time scale of about 64 days are noticeable in the power spectrum of the simulation results, which are not present in observational data. This indicates that the ParFlow-CLM model produced artefacts in the soil moisture simulation at a time scale of about 64 days. These artefacts are coincident with the dry periods as already discussed in Chapter 3.3.

At all depths, soil moisture was simulated by ParFlow-CLM with high coherence between August 2011 to June 2012 at a time scale of 64 days as well as 128 days almost without delay (Figs. 11, 12, and 14). Also for the period from July 2011 to March 2012, which is characterized by generally higher soil saturations, good agreement between simulated and observed soil moisture time series can be found (R^2: ~0.9). This indicates that the ParFlow-CLM model was better able to reproduce soil moisture dynamics during wet conditions.

4. Conclusions

We applied the 3-D hydrological model Parflow-CLM to the forested headwater catchment Wüstebach. We tested different parameterization strategies with respect to soil properties taking the anisotropy of K_s and the heterogeneity of soil porosity as examples. Finally, we explored the methods of EOF and cross-wavelet coherence for an in-depth analysis of our model results.

We found that scaling factor of 20 for the horizontal K_s of the soil layer that overlies the impermeable bedrock increased the model performance in terms of runoff and soil moisture dynamics, but not for ET. This indicates that the interflow process plays an important role for the generation of runoff in the Wüstebach catchment. Furthermore, we could show that spatial information on porosity can significantly improve the simulation of spatial pattern of soil moisture using a 3D hydrological model.

Our EOF analysis showed that the spatial pattern of observed soil moisture content is better reproduced by the ParFlow-CLM model with distributed soil porosity information used. However, given the limited heterogeneity in the input parameters, the spatial variability of simulated soil moisture was clearly lower compared to the observations. Nevertheless, the EOF analysis indicated the ParFlow-CLM model was able to reproduce a characteristic turning point θ_t as already found in the study by Graf et al. (2014), suggesting different spatial soil moisture pattern for mean soil moisture below and above θ_t.

Using the cross-wavelet coherence analysis we were able to analyze the model results in more detail. For instance, the analyses revealed that the ParFlow-CLM model can reproduce the soil moisture observations better during wet seasons. Dry seasons were suffered from delays of correlation and even anti-correlation between simulated and observed soil moisture.

Our detailed analysis of the ParFlow-CLM model results reveals a general overestimated of soil moisture content during dry seasons. We attribute this shortcoming to the low topographic gradients of the riparian zone that may have led to an underestimation of lateral drainage and thus overestimation of riparian zone wetness. Another possible reason is the presence of fast vertical bypass flow during strong precipitation events at the Wüstebach catchment, which cannot be considered by ParFlow-CLM.

Future studies should consider heterogeneous hydraulic parameters to increase the model performance. Such information could be generated by 3-D inverse calibration, which is, however, not feasible at the moment because of computational constraints. In addition, higher spatial resolution could help to reduce low topographic gradients effect in flat area like riparian zones. The effect of terrain on ParFlow simulation results was not regarded in this study and but should be investigated in future studies. Finally, by enhancing the ParFlow-CLM to consider by-pass flow during infiltration, a better agreement of the soil moisture simulation during dry periods could be achieved.

Acknowledgements

The authors would like to appreciate the support of project MIKLIP for this research. This work was also supported by the German Science Foundation (DFG) Transregional Collaborative Research Centre SFB/TR32: Patterns in Soil-Vegetation-Atmo sphere-Systems and the Helmholtz Society initiative TERENO (Terrestrial Environmental Observatories). The authors also would like to acknowledge the support of Centre for High-Performance Scientific Computing in Terrestrial Systems, HPSC TerrSys, Geoverbund ABC/J for their allocation of computer time for conducting numerical simulations. Crosswavelet and wavelet coherence software were provided by A. Grinsted.

References

Allen, R.G., Pereira, L.S., Raes, D., Smith, M., 1998. Crop Evapotranspiration: Guidelines for Computing crop Water Requirements. Food and Agriculture Organization of the United Nations, Rome.

Ashby, S.F., Falgout, R.D., 1996. A parallel miltugrid preconditioned conjugate gradient algorithm for groundwater flow simulations. Nucl. Sci. Eng. 124 (1), 145–159.

Bachmair, S., Weiler, M., 2012. Hillslope characteristics as controls of subsurface flow variability. Hydrol. Earth Syst. Sci. 16, 3699–3715.

Bogena, H.R., Herbst, M., Huisman, J.A., Rosenbaum, U., Weuthen, A., Vereecken, H., 2010. Potential of wireless sensor networks for measuring soil moisture variability. Vadose Zone J. 9 (4), 1002–1013.

Bogena, H.R., Huisman, J.A., Baatz, R., Hendricks-Franssen, H.-J., Vereecken, H., 2013. Accuracy of the cosmic-ray soil moisture probe in humid forest ecosystems: the worst case scenario. Water Resour. Res. 49, 1–14.

Bogena, H.R. et al., 2015. A terrestrial observatory approach for the integrated investigation of the effects of deforestation on water, energy, and matter fluxes. Sci. China Earth Sci. http://dx.doi.org/10.1007/s11430-014-4911-7.

Cornelissen, T., Diekkrüger, B., Bogena, H.R., 2014. Importance of a bedrock aquifer in the 3D simulation of discharge and soil moisture patterns at different spatial and temporal scales – the Wüstebach case study. J. Hydrol. 516, 140–153.

Dai, Y., Zeng, X., Dickinson, R.E., Baker, I., Bonan, G.B., Bosilovich, M.G., Denning, A.S., Dirmeyer, P.A., Houser, P.R., Niu, G., Oleson, K.W., Schlosser, C.A., Yang, Z.-L., 2003. The Common Land Model. Bull. Amer. Meteor. Soc. 84, 1013–1023.

Duan, Q., Sorooshian, S., Gupta, V.K., 1994. Optimal use of the SCE-UA global optimization method for calibrating watershed models. J. Hydrol. 158, 265–284.
Etmann, M. 2009. Dendrologische Aufnahmen im Wassereinzugsgebiet Oberer Wüstebach anhand verschiedener Mess-und Schätzverfahren. Master Thesis. Münster: University of Münster, 80.
Feddes, R.A., Kowalik, P., Kolinska-Malinka, K., Zaradny, H., 1976. Simulation of field water uptake by plants using a soil water dependent root extraction function. J. Hydrol. 31, 13–26.
Ghasemizade, M., Schirmer, M., 2013. Subsurface flow contribution in the hydrological cycle: lessons learned and challenges ahead—a review. Environ. Earth Sci. 69, 707–718.
Graf, A., Bogena, H.R., Drüe, C., Hardelauf, H., Pütz, T., Heinemann, G., Vereecken, H., 2014. Spatiotemporal relations between water budget components and soil moisture in a forested tributary catchment. Water Resour. Res. http://dx.doi.org/10.1002/2013WR014516.
Grinsted, A., Moore, J.C., Jevrejeva, S., 2004. Application of the cross wavelet transform and wavelet coherence to geophysical time series. Nonlin. Process. Geophys. 11, 561–566.
Groffman, P.M., Williams, C.O., Pouyat, R.V., Band, L.E., Yesilonis, I., 2009. Nitrate leaching and nitrous oxide flux in urban forests and grasslands. J. Environ. Qual. 38, 1848–1860.
Hopp, L., McDonnell, J.J., 2009. Connectivity at the hillslope scale: Identifying interactions between storm size, bedrock permeability, slope angle and soil depth. J. Hydrol. 376 (3–4), 378–391.
Hopp, L., McDonnell, J., Condon, P., 2011. Lateral subsurface flow in a soil cover over waste rock in a humid temperate environment. Vadose Zone J. 10. http://dx.doi.org/10.2136/vzj2010.0094.
Jawson, S.D., Niemann, J.D., 2007. Spatial patterns from EOF analysis of soil moisture at a large scale and their dependence on soil, land-use, and topographic properties. Adv. Water Resour. 30, 366–381.
Kim, G., Barros, A.P., 2002. Space–time characterization of soil moisture from passive microwave remotely sensed imagery and ancillary data. Remote Sens. Environ. 81, 93–403.
Koch, J., Jensen, K.H., Stisen, S., 2015. Toward a true spatial model evaluation in distributed hydrological modeling: Kappa statistics, Fuzzy theory, and EOF-analysis benchmarked by the human perception and evaluated against a modeling case study. Water Resour. Res.
Kollet, S., Maxwell, R.M., 2008. Capturing the influence of groundwater dynamics on land surface processes using an integrated, distributed watershed model. Water Resour. Res. 44 (W02402).
Lauzon, N., Anctil, F., Petrinovic, J., 2004. Characterization of soil moisture conditions at temporal scales from a few days to annual. Hydrol. Process. 18, 3235–3254.
Lin, H., 2006. Temporal stability of soil moisture spatial pattern and subsurface preferential flow pathways in the Shale Hills Catchment. Vadose Zone J. 5, 317–340.
Liu, Y., 2003. Spatial patterns of soil moisture connected to monthly-seasonal precipitation variability in a monsoon region. J. Geophys. Res. 108 (D22), 8856. http://dx.doi.org/10.1029/2002JD003124.
Mascaro, G., Vivoni, E.R., Méndez-Barroso, L.A., 2015. Hyperresolution hydrologic modeling in a regional watershed and its interpretation using empirical orthogonal functions. Adv. Water Resour. http://dx.doi.org/10.1016/j.advwatres.2015.05.023, ISSN 0309-1708.
Mauder, M., Desjardins, R.L., Oncley, S.P., MacPherson, I., 2007. Atmospheric response to a partial solar eclipse over a cotton field in central California. J. Appl. Meteorol. Climatol. 46, 1792–1803.
Maxwell, R.M., 2013. A terrain-following grid transform and preconditioner for parallel, large-scale integrated hydrologic modeling. Adv. Water Resour. 53, 109–117.
Maxwell, R.M., Kollet, S.J., Smith, S.G., Woodward, C.S., Falgout, R.D., Ferguson, I.M., Baldwin, C., Bosl, W.J., Hornung, R., Ashby, S., 2014. ParFlow User's Manual. International Ground Water Modeling Center Report GWMI 2010-01, 132p.
Maxwell, R.M., Miller, N.L., 2005. Development of a coupled land surface and groundwater model. J. Hydrometeorol. 6, 233–247.
Parent, A.C., Anctil, F., Parent, L.E., 2006. Characterization of temporal variability in near-surface soil moisture at scales from 1 h to 2 weeks. J. Hydrol. 325, 56–66.
Perry, M.A., Niemann, J.D., 2008. Generation of soil moisture patterns at the catchment scale by EOF interpolation. Hydrol. Earth Syst. Sci. 12, 39–53.
Qu, W., Bogena, H.R., Huisman, J.A., Martinez, G., Pachepsky, Y.A., Vereecken, H., 2014. Effects of soil hydraulic properties on the spatial variability of soil moisture: evidence from sensor network data and inverse modeling. Vadose Zone J. http://dx.doi.org/10.2136/vzj2014.07.0099.
Rahman, M., Sulis, M., Kollet, S.J., 2014. The concept of dual-boundary forcing in land surface-subsurface interactions of the terrestrial hydrological and energy cycles. Water Resour. Res. http://dx.doi.org/10.1002/2014WR015738.
Richter, D., 1995. Ergebnisse methodischer Untersuchungen zur Korrektur des systematische Mesfehlers des Hellmann-Niederschlagmessers. In Berichte des Deutschen Wetterdienstes. 194, Lysimeter Research Group, Selbstverlag des Deutschen Wetterdienstes, Offenbach am Main, Germany. pp. 93.
Rosenbaum, U., Bogena, H.R., Herbst, M., et al., 2012. Seasonal and event dynamics of spatial soil moisture patterns at the small catchment scale. Water Resour. Res. 48, W10544. http://dx.doi.org/10.1029/2011WR011518.
Schaap, M., Bouten, W., Verstraten, J., 1997. Forest floor moisture dynamics in a Douglas fir stand. J. Hydrol. 201, 367–383.
Schaefli, B., Zehe, E., 2009. Hydrological model performance and parameter estimation in the wavelet-domain. Hydrol. Earth Syst. Sci. 13, 1921–1936.
Schmidt, R., Petrovic, S., Güntner, A., Barthelmes, F., Wünsch, J., Kusche, J., 2008. Periodic components of water storage changes from GRACE and global hydrology models. J. Geophys. Res. 113, B08419. http://dx.doi.org/10.1029/2007JB005363.
Si, B.C., 2008. Spatial scaling analyses of soil physical properties: a review of spectral and wavelet methods. Vadose Zone J. 7, 547–562.
Simmer, C. et al., 2015. Monitoring and modeling the terrestrial system from pores to catchments - the transregional collaborative research center on patterns in the Soil-VegetationAtmosphere System. Bulletin of the American Meteorological Society. http://dx.doi.org/10.1175/BAMS-D-13-00134.1.
Simunek, J., van Genuchten, M.Th., 2008. Modeling nonequilibrium flow and transport processes using HYDRUS. Vadose Zone J. 7 (2), 782–797.
Stockinger, M., Bogena, H., Lücke, A., Diekkrüger, B., Weiler, M., Vereecken, H., 2014. Seasonal soil moisture patterns control transit time distributions in a forested headwater catchment. Water Resour. Res. 50. http://dx.doi.org/10.1002/2013WR014815.
Syed, T.H., Lakshmi, V., Paleologos, E., Lohmann, D., Mitchell, K., Famiglietti, J.S., 2004. Analysis of process controls in land surface hydrological cycle over the continental United States. J. Geophys. Res. 109, D22105.
Tang, K.M., McGinnis, D.F., Frindte, K., Brüchert, V., Grossart, H.P., 2014. Paradox reconsidered: methane oversaturation in well-oxygenated lake waters. Limnol. Oceanogr. 59, 275–284.
TERENO, 2011. Forschungszentrum Jülich, Jülich, Germny. Available at <http://teodoor.icg.kfa-juelich.de/> (verified 09.10.12).
Torrence, C., Compo, G.P., 1998. A practical guide to wavelet analysis. Bull. Am. Meteorol. Soc. 79, 61–78.
Tromp-van Meerveld, H.J., McDonnell, J.J., 2006. Threshold relations in subsurface stormflow 2: The fill and spill hypothesis. Water Resour. Res. 42, W02411.
Uchida, T., Tromp-van Meerveld, I., McDonnell, J.J., 2005. The role of lateral pipe flow in hillslope runoff response: an intercomparison of non-linear hillslope response. J. Hydrol. 311 (1–4), 117–133.
Vargas, R., Detto, M., Baldocchi, D.D., Allen, M.F., 2010. Multiscale analysis of temporal variability of soil CO_2 production as influenced by weather and vegetation. Glob. Change Biol. 16, 1589–1605.
Vrugt, J.A., Gupta, H.V., Bouten, W., Sorooshian, S., 2003. A Shuffled Complex Evolution Metropolis algorithm for optimization and uncertainty assessment of hydrologic model parameters. Water Resour. Res. 39 (8), 1201.
Weiler, M., McDonnell, J.J., 2007. Conceptualizing lateral preferential flow and flow networks and simulating the effects on gauged and ungauged hillslopes. Water Resour. Res. 43, W03403.
Wiekenkamp, I., Huisman, J.A., Bogena, H., Lin, H., Vereecken, H., 2015. Spatial and temporal occurrence of preferential flow at the catchment scale. J. Hydrol., submitted for publication.
Wood, E.F. et al., 2011. Hyper-resolution global land surface modeling: meeting a grand challenge for monitoring Earth's terrestrial water. Water Resour. Res. 47, W05301.
Zacharias, S., Bogena, H., Samaniego, L., Mauder, M., Fuß, R., Pütz, T., Frenzel, M., Schwank, M., Baessler, C., Butterbach-Bahl, K., Bens, O., Borg, E., Brauer, A., Dietrich, P., Hajnsek, I., Helle, G., Kiese, R., Kunstmann, H., Klotz, S., Munch, J.C., Papen, H., Priesack, E., Schmid, H.P., Steinbrecher, R., Rosenbaum, U., Teutsch, G., Vereecken, H., 2011. A network of terrestrial environmental observatories in Germany. Vadose Zone J. 10 (3), 955–973.
Zhang, Z.F., Ward, A.L., Gee, G.W., 2004. A combined parameter scaling and inverse technique to upscale the unsaturated hydraulic parameters for heterogeneous soils. Water Resour. Res., W08306
Zhang, B., Tang, J., Gao, C., Zepp, H., 2011. Subsurface lateral flow from hillslope and its contribution to nitrate loading in streams through an agricultural catchment during subtropical rainstorm events. Hydrol. Earth Syst. Sci. 15, 3153–3170.